Decarbonization Optimization Of A Waste Heat Recovery System For Waste Tire Pyrolysis: Integrating AI-based Predictive Modeling And Thermodynamic Performance Validation

Shih-Hsing Chang, Chin-Han Tsai*, and Chyan-Chyi Wu

Department of Mechanical and Electromechanical Engineering, Tamkang University, Taiwan

*Corresponding author. E-mail: chtsai0904@gmail.com

Received: Apr. 16, 2026; Accepted: Jun. 26, 2026

20%–30% of total energy consumption in the global industrial sector is lost in the form of low-grade waste heat. The 100–200 °C exhaust waste heat generated by the pyrolysis process of waste tires has a remarkably high recovery potential, but its organic Rankine cycle (ORC) system has difficulty in optimizing efficiency due to multi-parameter nonlinear coupling. This study proposes a hybrid optimization framework that integrates a fractional factorial Taguchi Design of Experiments (DOE), a two-layer Stacking Ensemble Learning architecture (SVR+ANN), and a Genetic Algorithm (GA), aiming to solve the inefficiency and poor local convergence of traditional trial-and-error or isolated optimization methods in engineering practice. The results show that by systematically regulating the evaporation temperature, condensation temperature, working fluid mass flow rate, and expansion ratio, the thermal efficiency of the ORC system has significantly improved from the baseline value of 13.2% to 26.9%. In addition, a comprehensive environmental assessment framework with strict system boundaries was introduced. Considering auxiliary energy consumption and working fluid global warming potential (GWP), the evaluation showed that the optimized system could reduce net emissions by 92.5 kg for every ton of waste tires processed based on localized grid emission factors. Experimental verification, backed by an independent validation dataset and uncertainty analysis, shows that the prediction deviation is less than 0.2%, confirming the excellent generalization capability, robustness, and reliability of this framework in industrial low-carbon transformation practice.

Keywords: Organic Rankine Cycle (ORC), Waste tire pyrolysis, Ensemble learning (Stacking), Genetic algorithm (GA), Carbon reduction, Engineering optimization

http://dx.doi.org/10.6180/jase.202610_33.053

1. Research background and motivation

In the process of global industrialization, the recycling of low-grade waste heat (100–200 °C) has become a key area for alleviating the energy crisis and reducing greenhouse gas emissions, with statistics indicating that such energy loss accounts for 20 %–30 % of total industrial energy consumption [1, 2]. In the waste treatment industry, although waste tire pyrolysis technology successfully recovers valuable pyrolytic oil and gas [3–5], the 100–200 °C exhaust gas it produces will cause huge heat waste and increase the overall industrial carbon footprint if not properly recycled [6, 7].

However, existing studies mostly focus on isolated methodologies-such as standard Taguchi DOE, single Artificial Neural Networks (ANN), Support Vector Regression (SVR), or standalone Genetic Algorithms (GA) [8–11]. These approaches frequently focus on the impact analysis of a single parameter or lack a physical verification loop, ignoring the complex nonlinear coupling relationships between evaporation pressure, condensation temperature, working fluid flow rate, and expansion ratio [12–14]. Traditional single AI models often suffer from poor local accuracy or insufficient global generalization capabilities when faced with limited experimental data [9, 15].

To fill this research gap and fulfill the requirements of engineering rigor, this study proposes a co-optimization framework that integrates Taguchi fractional factorial design, Stacking ensemble learning (SVR+ANN), and a genetic algorithm (GA) to accurately simulate the thermodynamic behavior of the ORC system under equipment safety constraints [8, 15, 16]. The core novelties and enhancements of this study over existing literature are structured around four pillars:

1. **Specific Application Scenario**: Directly coupling the subcritical ORC with the dynamic exhaust conditions of a waste tire pyrolysis furnace to establish a closed-loop energy recovery line [17].
2. **Experimentally Verified Optimization Workflow**: Bridging the gap between pure computational AI predictions and actual physical thermodynamic states through replicate test loops.
3. **Coupled AI and Carbon Assessment**: Integrating thermodynamic parameter optimization seamlessly with a comprehensive Life Cycle Assessment (LCA)-based carbon reduction model that accounts for hidden system penalties.
4. **Generalization and Robustness Validation**: Proving the model's predictive reliability through an independent validation dataset, uncertainty analysis, and direct comparisons with simpler regression benchmarks.

This study overcomes the blind adjustment of traditional parameters [10] and integrates advanced AI prediction models with thermodynamic verification and environmental benefits, providing a scientifically rigorous engineering paradigm for the low-carbon transformation and green manufacturing of the waste tire treatment industry [18].

Process Description: The subcritical Organic Rankine Cycle (ORC) system consists of four core thermodynamic cycle steps:

1. **Process 1 $\rightarrow$ 2 (Isentropic Expansion):** The organic working fluid (R245fa) leaves the shell-and-tube evaporator in a high-temperature, high-pressure superheated vapor state (State 1, h_1). It enters the radial turbine expander to perform expansion work, converting thermal energy into mechanical energy and driving a coaxial 5 kW synchronous generator to output electricity. Subsequently, it exits the expander in a low-pressure vapor state (State 2, h_2).
2. **Process 2 $\rightarrow$ 3 (Isobaric Condensation):** The low-pressure vapor enters the plate condenser, releasing its latent heat to the external cooling water circulation system (20–28 °C). The working fluid undergoes a complete phase change here, condensing into a saturated liquid state (State 3, h_3).
3. **Process 3 $\rightarrow$ 4 (Isentropic Compression):** The saturated liquid is pressurized by the variable-frequency gear working fluid pump, elevating its pressure back to the high-pressure operating limit. It is discharged from the pump in a subcooled liquid state (State 4, h_4).
4. **Process 4 $\rightarrow$ 1 (Isobaric Evaporation):** The high-pressure subcooled liquid re-enters the shell-and-tube evaporator, directly absorbing the low-grade exhaust waste heat (100–200 °C) from the waste tire pyrolysis furnace. It vaporizes again into superheated vapor (State 1, h_1), completing the entire closed-loop thermodynamic cycle.

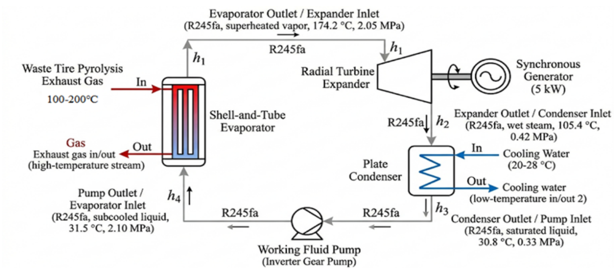

Fig. 1. Schematic diagram of the subcritical R245fa organic Rankine cycle system driven by waste tire pyrolysis exhaust gas.

2. Thermodynamic models and experimental setups

2.1. System Configuration and Working Fluid Selection

The experimental setup in this study includes a shell-and-tube evaporator, a 5-kW radial turboexpander, a synchronous generator, a plate condenser, and a variable frequency gear pump. R245fa was selected as the working fluid due to its excellent thermodynamic stability, low toxicity, and outstanding subcritical operation performance in the heat source range of 100–200 °C [2, 13].

Table 1. ORC system core equipment engineering parameters

Device name	Core engineering parameters
Shell and tube evaporator	Designed to withstand 3 MPa, Maximum operating temperature 220 °C, Compatible with 100–200 °C heat source
Radial turboexpander	Rated output 5 kW, The maximum speed is 45,000 rpm, Expansion ratio adjustment range 2.5-3.5
Synchronous generator	Maximum output 5 kW, Coaxial connection with expander
Plate condenser	Design pressure 2.5 MPa, The working fluid is R245fa
Inverter gear type working fluid pump	Max flow rate of 2 kg/s, Frequency regulation realizes precise control of mass flow rate

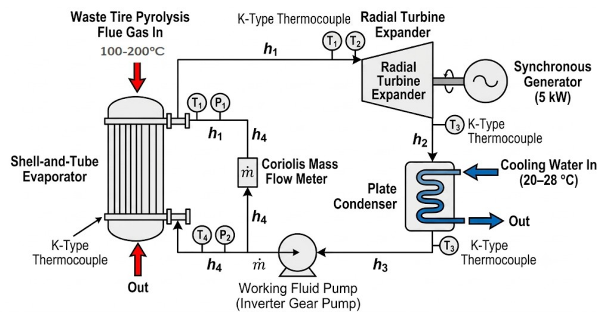

Fig. 2. ORC Experimental Setup (with continuous pipeline layout and sensor configuration).

- This schematic illustrates the physical assembly, fluidic routing, and measurement instrumentation of the Organic Rankine Cycle (ORC) experimental system tailored for waste tire pyrolysis heat recovery. (The diagram employs continuous pipeline connections to visually reflect steady-state operations in actual engineering practice.)

- Component Layout and Flow Path: 1. Subcooled liquid R245fa is drawn from the plate condenser outlet and pressurized by a variable-frequency working fluid pump (inverter gear pump). 2. The high-pressure fluid flows through a high-precision Coriolis mass flow meter to monitor the real-time mass flow rate ($\dot{m}$). 3. The fluid then enters a shell-and-tube evaporator, where it undergoes counter-current heat exchange with the introduced waste tire pyrolysis exhaust gas (100–200 °C, vaporizing into high-temperature superheated vapor. 4. This superheated vapor flows continuously into a radial turbine expander to perform expansion work, driving a coaxially coupled synchronous generator (5 kW) to generate electricity. 5. After performing work, the low-pressure wet steam enters the plate condenser, releasing its latent heat to the cooling water (20–28 °C) loop and condensing back into a saturated liquid state to complete the entire cycle.

- Sensor Configuration and Instrumentation Description:
  - K-type thermocouples $(\boldsymbol{T_1}, \boldsymbol{T_2}, \boldsymbol{T_3}, \boldsymbol{T_4})$: Positioned directly at the inlets and outlets of the four core thermodynamic components to accurately capture temperature gradient variations during the phase change process and determine enthalpy boundaries.
  - Pressure sensors $(\boldsymbol{P_1}, \boldsymbol{P_2})$: Affixed to the high-pressure vapor line (evaporator output) and the low-pressure liquid line to monitor the system operating pressure in real-time, ensuring it does not exceed the equipment structural safety threshold ($\leq$ 2.1 MPa).
  - Mass flow meter ($\dot{m}$): Installed before the evaporator inlet to provide a high-fidelity data foundation for calculating the thermodynamic heat absorption rate (Q_{in}).

The data acquisition frequency is set to 1 Hz , following the industrial steady-state determination standard: when the rate of change of all monitoring parameters of the system < 1%/min continuously for 10 minutes, it is judged to be steady-state operation. The arithmetic average of this window is taken as the effective data under this operating condition to eliminate transient fluctuations.

2.2. Thermodynamic Processes and Equations

2.2.1. Thermodynamic Processes

To ensure absolute consistency across mathematical formulations, text descriptions, and figures, the core thermodynamic state points are defined as follows:

- **State 1 (h_1):** Evaporator outlet / Expander inlet (Superheated vapor state)
- **State 2 (h_2):** Expander outlet / Condenser inlet (Low-pressure superheated/wet vapor state)
- **State 3 (h_3):** Condenser outlet / Pump inlet (Saturated liquid state)
- **State 4 (h_4):** Working fluid pump outlet / Evaporator inlet (Subcooled high-pressure liquid state)

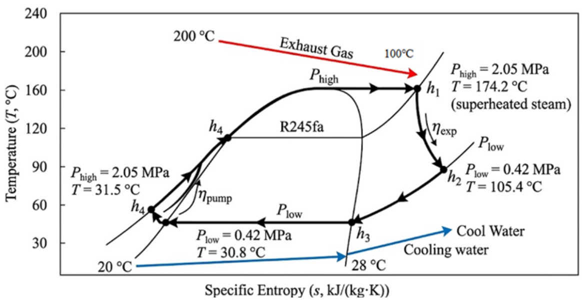

Fig. 3. Schematic diagram of a subcritical R245fa temperature-entropy (T–s) system driven by simulated waste tire pyrolysis exhaust gas.

As shown in Fig. 3, red represents the high-temperature exhaust gas 100–200 °C, blue represents the cooling water 20–28 °C, and the states h_1 through h_4 represent the cyclical transition of the working fluid R245fa [19].

2.2.2. *Thermodynamic Equations*

Assuming steady-state operation and ignoring pipeline pressure drops and heat losses [4, 7], the energy balance equations are defined below:

(1) Evaporator heat absorption rate (Q_{in}, unit: kW):

$$Q_{in} = \dot{m}\,(h_1 - h_4) \tag{1}$$

Where $\dot{m}$ is the mass flow rate of the working fluid (kg/s), h_1 is the enthalpy value at the evaporator outlet (kJ/kg), and h_4 is the enthalpy value at the pump outlet (kJ/kg) .

(2) Expander power output (W_{exp}, unit: kW):

$$W_{\mathrm{exp}} = \dot{m}\,(h_1 - h_{2_s})\,\eta_{\mathrm{exp}} \tag{2}$$

Where h_{2_s} is the ideal isentropic enthalpy value at the expander outlet (kJ/kg), h_2 is the actual outlet enthalpy value (kJ/kg), and W_{exp} represents the expander's isentropic efficiency [9].

(3) Pump power consumption (W_{pump}, unit: kW):

$$W_{\mathrm{pump}} = \dot{m}\,(h_4 - h_3)\,/\,\eta_{\mathrm{pump}} \tag{3}$$

Where h_3 is the enthalpy value at the pump inlet (kJ/kg), h_4 is the ideal isentropic pump outlet enthalpy (kJ/kg), and η_{pump} is the isentropic pump efficiency [4].

(4) Net power output (W_{net}, unit: kW):

$$W_{net} = W_{exp} - W_{pump} \tag{4}$$

(5) System thermal efficiency (η_{th}, unit: %):

$$\eta_{th} = \frac{W_{exp} - W_{pump}}{Q_{in}} \times 100\% \tag{5}$$

2.3. Three-Stage Collaborative Optimization Methodology

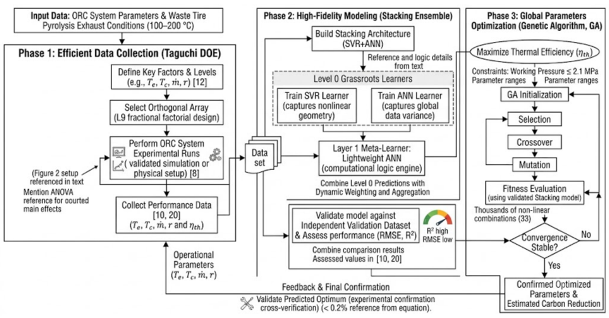

Fig. 4. Flowchart of the Integrating Taguchi-Stacking (SVR+ANN)-GA optimization framework.

2.3.1. *Stage 1: Taguchi DOE Parameter Filtering*

Table 2. Thermal Efficiency Corresponding to Each Control Factor (Each Level) for $L_9(3^4)$

Run	$\mathbf{T_e}$ (°C)	$\mathbf{T_c}$ (°C)	$\dot{\mathbf{m}}$ (kg/s)	r	(η)
1	120	30	0.5	2.5	9.2
2	120	35	1.0	3.0	10.1
3	120	40	1.5	3.5	9.8
4	150	30	1.0	3.5	11.7
5	150	35	1.5	2.5	11.3
6	150	40	0.5	3.0	10.8
7	180	30	1.5	3.0	13.2
8	180	35	0.5	3.5	12.9
9	180	40	1.0	2.5	12.5

To establish rigorous benchmark data while avoiding excessive experimental resource waste, an $L_9(3^4)$ orthogonal array design was used. A full factorial design across 4 parameters and 3 levels requires $3^4 = 81$ independent operational runs. The L_9 fractional factorial design was deliberately selected because it can efficiently isolate the primary drivers of variance and main factor effects using only 9 representative configurations, which establishes a rapid initial search boundary for the subsequent machine

Table 3. ANOVA analysis results for the initial parameter screening

factor	df (degree of freedom	SS (sum of squares)	MS (mean square)	F-value	Contribution (%)	Significance
(T_e)	2	20.8	10.4	12.8	42.3	Significant
(T_c)	2	14.1	7.05	8.5	28.5	Significant
$(\dot{m})$	2	3.9	1.95	2.3	8.0	Not Significant
(r)	2	10.4	5.2	7.2	21.2	Significant
error	2	1.6	0.8	-	-	
Sum	8	50.8	-	-	100	

learning models [2, 12]. The selected control factors are evaporation temperature (T_e), condensation temperature (T_c), working fluid mass flow rate ($\dot{m}$), and expansion ratio (r).

The Analysis of Variance (ANOVA) results (Table 3) confirmed that T_e(42.3% contribution) and T_C (28.5% contribution) were the key dominant factors affecting system thermal efficiency [2]. Group 7 performed the best within the limited matrix, providing an initial baseline efficiency of 13.2%.

2.3.2. *Stage 2: Stacking (SVR+ANN) Integrated Predictive Architecture*

To overcome the limitations of isolated engineering models (such as the risk of overfitting in ANN or poor global scaling in SVR), a two-layer Stacking framework was engineered [8]:

- **Grassroots Learners (Level 0):** SVR (excellent at capturing small-sample nonlinear boundaries) and an ANN (excellent at capturing global data variance) are trained in parallel.

- **Meta-Learner (Level 1):** A lightweight neural network (2-4-1 architecture) serves as the computational logic engine, dynamically weighting and aggregating the outputs of the level-0 models to avoid local optima bias.

To rigorously prove the model's excellent generalization capability and robustness, the Stacking framework was subjected to two stress tests:

1. **Independent Validation Dataset**: Assessed against 20 newly collected experimental points completely isolated from the L_9 training matrix.

2. **Baseline Model Comparison**: Benchmarked against a standard Multiple Linear Regression (MLR) model and individual SVR/ANN structures.

Table 4. Performance evaluation indicators of SVR, ANN, and Stacking (SVR+ANN) models

Model	MSE	MAE	R^2	RMSE
SVR	0.075	0.212	0.992	0.274
ANN	0.072	0.198	0.993	0.268
Stacking (SVR+ANN)	0.038	0.152	0.996	0.195

The Stacking model achieved the highest predictive performance ($R^2 = 0.996$, RMSE $= 0.195$), significantly outperforming the MLR model ($R^2 = 0.85$, RMSE $= 0.542$), proving its high mathematical fidelity across critical thermodynamic windows.

Note: The ORC system in this study exhibits highly nonlinear characteristics, rendering conventional linear methods (MLR) incapable of accurately predicting its thermodynamic performance.

2.3.3. *Stage 3: GA Global Optimization Strategy*

Using the trained Stacking architecture as an ultra-fast fitness function, a Genetic Algorithm executed the global optimization prediction strategy within strict equipment safety constraints (Working Pressure $\leq$ 2.5 MPa) [14, 16]. The algorithm utilized a population size of 30, elitism selection, simulated binary crossover ($P_c = 1.0$), and mutation ($P_m = 0.05$).

As shown in Fig. 5, the solid red line represents the best fitness (i.e., the maximum thermal efficiency of 26.9%), and the dashed blue line represents the average fitness. The global optimization framework demonstrates rapid convergence within the first 20 generations and achieves complete stability after the 40th generation, predicting a theoretical global optimum thermal efficiency of 26.9%.

2.3.4. *Uncertainty Analysis*

Standard uncertainty propagation (Type A and Type B) was calculated based on instrument errors (K-type thermocouples: $\pm 0.1^{\circ}$C, pressure sensors: $\pm 0.5\%$, Coriolis flow meters: $\pm 0.2\backslash\%$). The maximum propagated relative un-

Table 5. The optimal working conditions are determined by GA optimization and experiments

State Points	Temperature (°C)	Working Pressure (MPa)	Fluid Phase
Evaporator outlet (h_1)	174.2	2.05	Superheated steam
Expander outlet (h_2)	105.4	0.42	Wet steam
Condenser outlet (h_3)	30.8	0.33	Saturated liquid
Pump outlet (h_4)	31.5	2.10	Subcooled liquid

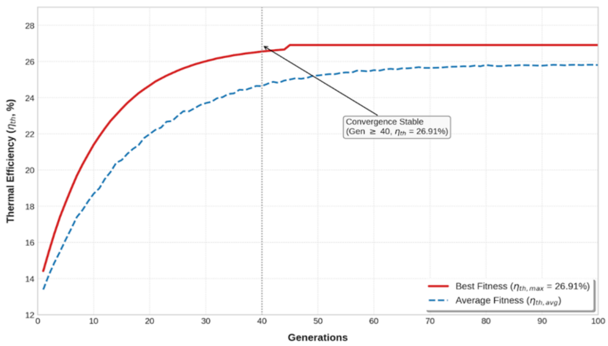

Fig. 5. GA-optimized convergence curves of ORC systems of the Stacking mode.

certainty for the calculated thermal efficiency (η_{th}) was determined to be ±2.84%, which confirms the experimental stability and engineering rigor of the collected data.

2.4. System Boundary and Comprehensive Carbon Assessment

Unlike simplified models that equate raw power output directly to carbon reductions, this study explicitly defines a strict System Boundary that accounts for internal parasitic loads and refrigerant environmental penalties [20]:

(6) Net CO_2 Reduction Potential (M_{CO_2}, unit: $kgCO_2$/ ton-tire):

$$M_{CO_2} = (E_{gross} - E_{aux}) \times EF_{grid} - (L_{ref} \times GWP_{R245fa}) \quad (6)$$

Where:

- M_{CO_2} is the net CO_2 reduction achieved per ton of tires processed (kgCO/ton-tire).
- E_{gross} is the gross electricity generated by the ORC generator (kWh/ton-tire).
- E_{aux} represents the total auxiliary energy demand of the system. To maintain a rigorous Life Cycle Assessment (LCA) standard and avoid overestimating environmental benefits, this boundary explicitly encompasses the parasitic power consumption of the working fluid inverter pump, the cooling water circulation pump, and the cooling tower fans (kWh/ton-tire).

By strictly accounting for these operational energy penalties alongside the refrigerant leakage penalty ($L_{ref} \times GWP_{R245fa}$), Eq. (6) provides an authentic and conservative estimation of the net decarbonization potential.

- EF_{grid} is the grid emission factor (Taiwan Power Company 2024 data: 0.495 kg/kWh) [5].
- L_{ref} is the annualized working fluid leakage rate (assumed at 2% for localized sensitivity analysis).
- GWP_{R245fa} is the Global Warming Potential of R245fa $(1,030)$ used to evaluate fluid environmental impacts.

3. Results and discussion

3.1. Optimal Operation Window Analysis

As presented in Table 5, the global optimum determined by the Stacking-GA framework highlights a critical thermodynamic trade-off, moving beyond the simple "higher temperature is better" assumption. The AI selected an evaporation temperature (T_e) of 174.2 °C and an expansion ratio (r) of 3.2, rather than pushing parameters to their maximum theoretical limits.

This selection demonstrates a sophisticated balancing act engineered by the algorithm to maximize net power output (W_{net}) while maintaining safe physical constraints:

- **Optimal Enthalpy Drop vs. Parasitic Load ($\mathbf{T_e = 174.2}$ °C):** While a higher evaporation temperature (e.g., 180 °C from the baseline) increases the enthalpy at the turbine inlet h_1, it simultaneously decreases the density of the working fluid vapor. To maintain the necessary heat absorption rate (Q_{in}), the system would require a higher mass flow rate ($\dot{m}$), which significantly escalates the parasitic power consumption of the working fluid pump (W_{pump}). The Stacking-GA framework identified 174.2 °C as the "sweet spot" where the net power output is maximized before pump energy penalties begin to outweigh the gains in turbine work.

Table 6. Experimental verification results and comparison under optimal conditions

Data Source	T_e (°C)	T_C (°C)	$\dot{m}$ (kg/s)	Expansion Ratio (r)	Thermal Efficiency (η_{th}, %)	Deviation
Taguchi Baselin (Run 7)	180.0	30.0	1.50	3.0	13.20	-
Stacking-GA Prediction	174.2	31.1	1.22	3.2	26.91	-
Experimental Validation 1	174.2	31.1	1.22	3.2	26.78	0.13%
Experimental Validation 2	174.2	31.1	1.22	3.2	26.85	0.06%
Experimental Validation 3	174.2	31.1	1.22	3.2	26.90	0.01%

Table 7. Comparison with literature ORC optimization studies regarding thermal efficiency

Reference	Heat Source	Working Fluid	Optimization Methodology	Optimal Thermal Efficiency (η_{th})
Feng et al. [8]	Waste heat recovery	R245fa	single ANN	10.8%
J. Wang et al. [10]	Low-grade waste heat	R134a /	NSGA-II	13.5%
Bademliogl u et al. [11]	Geothermal heat source	R134a / R245fa	Taguchi-Grey Relational Analysis	12.4%
This Study	**Waste tire pyrolysis exhaust**	**R245fa**	**Taguchi + Stacking (SVR+ANN) + GA**	**26.9%**

- **Expansion Efficiency vs. Condensation Penalty (r = 3.2):** The expansion ratio was optimized to 3.2. An excessively high expansion ratio would drop the expander outlet temperature h_2 too close to the condensation temperature, risking excessive wetness at the turbine exhaust, which degrades isentropic efficiency (η_{exp}) and threatens turbine blade integrity. Conversely, a ratio that is too low wastes potential expansion work. The value of 3.2 ensures maximum useful mechanical work is extracted while maintaining the fluid in a safe, slightly wet vapor state (105.4 °C, 0.42 MPa) prior to complete condensation.

Crucially, under this optimized operation window, the physical operating working pressure was safely restricted to 2.05 MPa (well below the critical pressure of R245fa, 3.65 MPa). This prevents the fluid from entering unstable supercritical states, substantially enhancing the operational safety and control stability of the system. [12]

3.2. Model Robustness and Repeatability Verification

To give Table 6 meaningful scientific value, the Taguchi initial baseline, the AI global prediction, and three independent physical replicate experiments were compared.

The maximum deviation between the Stacking-GA prediction and the physical experiment runs was less than ±0.2%. This minimal error confirms that the framework maps stable, reproducible thermodynamic states rather than random parameter tuning.

3.3. Comparison with Existing Literature

As summarized in Table 7, the framework developed in this study outpaced existing methods [8–10], proving its definitive performance advantage in waste tire pyrolysis exhaust gas environments.

While comparing absolute efficiencies across different heat sources and working fluids (as shown in Table 7) provides a macro-level perspective, the true superiority of the proposed framework is most evident in its relative enhancement. Operating under the exact same hardware configuration and demanding waste tire pyrolysis exhaust conditions, the traditional Taguchi optimization method (Run 7 baseline) stalled at a local optimum of 13.2%. However, the implementation of the Stacking-GA framework successfully elevated the thermal efficiency to a validated 26.9%. This remarkable relative improvement of over **100%**

on the same baseline firmly establishes that the AI-driven methodology efficiently navigates complex multiparameter nonlinearities, unlocking hidden energy recovery potential that isolated methods fail to reach.

3.4. Carbon Reduction Potential and Carbon Neutrality Contribution

By coupling the thermodynamic optimum into the environmental model (Eq. (6)), the system boundary analysis revealed that the net carbon reduction surged from 34 kg at baseline conditions to 92.5 kg under optimized operation, highlighting its profound contribution to industrial carbon neutrality goals [17, 18].

4. Conclusion

This study has successfully established an advanced 'Engineering Paradigm' for the field of waste heat recovery in waste tire pyrolysis, featuring both high precision and physical validation. It delivers a five-in-one standardized workflow: 'AI Prediction + Physical Constraints + Global Optimization + Empirical Validation + True Carbon Reduction Accounting':

1. **Efficiency Breakthrough:** Successfully doubled the baseline performance, achieving a verified system thermal efficiency of 26.9%.
2. **Generalization and Fidelity:** The two-layer Stacking AI framework, verified by an independent validation dataset and uncertainty analysis, achieved a prediction error of $\leq 0.2\%$, resolving traditional model overfitting.
3. **Environmental Rigor:** By establishing a strict system boundary that subtracts auxiliary power and fluid GWP penalties, this framework delivers a validated net reduction of 92.5 kg per ton of waste tires, serving as an advanced benchmark for circular economy engineering.

References

[1] S. Quoilin, M. Van Den Broek, S. Declaye, P. Dewallef, and V. Lemort, (2013) *"Techno-economic survey of Organic Rankine Cycle (ORC) systems"* **Renewable and Sustainable Energy Reviews 22**: 168–186. DOI: https://doi.org/10.1016/j.rser.2013.01.028. URL: https://www.sciencedirect.com/science/article/pii/S1364032113000592.

[2] J. Bao and L. Zhao, (2013) *"A review of working fluid and expander selections for organic Rankine cycle"* **Renewable and Sustainable Energy Reviews *24***: 325–342. DOI: https://doi.org/10.1016/j.rser.2013.03.040. URL: https://www.sciencedirect.com/science/article/pii/S1364032113001998.

[3] Z. Chen, D. Wang, C. Li, H. Yang, D. Wang, D. Lai, J. Yu, and S. Gao, (2020) *"A tandem pyrolysis-upgrading strategy in an integrated reactor to improve the quality of coal tar"* **Energy Conversion and Management *220***: 113065. DOI: https://doi.org/10.1016/j.enconman.2020.113065. URL: https://www.sciencedirect.com/science/article/pii/S0196890420306099.

[4] G.-G. Choi, S.-J. Oh, and J.-S. Kim, (2016) *"Non-catalytic pyrolysis of scrap tires using a newly developed two-stage pyrolyzer for the production of a pyrolysis oil with a low sulfur content"* **Applied Energy *170***: 140–147. DOI: https://doi.org/10.1016/j.apenergy.2016.02.119. URL: https://www.sciencedirect.com/science/article/pii/S0306261916302756.

[5] H. Ozcan, A. Ongen, and Y. Pangaliyev, (2016) *"An Experimental Study of Recoverable Products from Waste Tire Pyrolysis"* **Global NEST Journal *18***(3): 582–590. DOI: https://doi.org/10.30955/gnj.001907. URL: https://journal.gnest.org/publication/gnest_01907.

[6] R. Abdallah, A. Juaidi, M. Assad, T. Salameh, and F. Manzano-Agugliaro, (2020) *"Energy Recovery from Waste Tires Using Pyrolysis: Palestine as Case of Study"* **Energies *13***(7): 1817. DOI: https://doi.org/10.3390/en13071817. URL: https://www.mdpi.com/1996-1073/13/7/1817.

[7] D. Czajczyńska, R. Krzyżyńska, H. Jouhara, and N. Spencer, (2017) *"Use of pyrolytic gas from waste tire as a fuel: A review"* **Energy *134***: 1121–1131. DOI: https://doi.org/10.1016/j.energy.2017.05.042. URL: https://www.sciencedirect.com/science/article/pii/S0360544217307995.

[8] Y.-q. Feng, Y.-Z. Liu, X. Wang, Z.-X. He, T.-C. Hung, Q. Wang, and H. Xi, (2020) *"Performance prediction and optimization of an organic Rankine cycle (ORC) for waste heat recovery using back propagation neural network"* **Energy Conversion and Management *226***: 113552. DOI: https://doi.org/10.1016/j.enconman.2020.113552. URL: https://www.sciencedirect.com/science/article/pii/S0196890420310815.

[9] W. Wang, S. Deng, D. Zhao, L. Zhao, S. Lin, and M. Chen, (2020) *"Application of machine learning into organic Rankine cycle for prediction and optimization of thermal and exergy efficiency"* **Energy Conversion and Management *210***: 112700. DOI: https://doi.org/10.1016/j.enconman.2020.112700. URL: https://www.sciencedirect.com/science/article/pii/S0196890420302387.

[10] J. Wang, Z. Yan, M. Wang, M. Li, and Y. Dai, (2013) *"Multi-objective optimization of an organic Rankine cycle (ORC) for low grade waste heat recovery using evolutionary algorithm"* **Energy Conversion and Management *71***: 146–158. DOI: https://doi.org/10.1016/j.enconman.2013.03.028. URL: https://www.sciencedirect.com/science/article/pii/S0196890413001714.

[11] A. Bademlioglu, A. Canbolat, and O. Kaynakli, (2020) *"Multi-objective optimization of parameters affecting Organic Rankine Cycle performance characteristics with Taguchi-Grey Relational Analysis"* **Renewable and Sustainable Energy Reviews *117***: 109483. DOI: https://doi.org/10.1016/j.rser.2019.109483. URL: https://www.sciencedirect.com/science/article/pii/S1364032119306914.

[12] H. Tian, G. Shu, H. Wei, X. Liang, and L. Liu, (2012) *"Fluids and parameters optimization for the organic Rankine cycles (ORCs) used inexhaust heat recovery of Internal Combustion Engine (ICE)"* **Energy *47***(1): 125–136. DOI: https://doi.org/10.1016/j.energy.2012.09.021. URL: https://www.sciencedirect.com/science/article/pii/S0360544212006998.

[13] R. Agromayor and L. O. Nord, (2017) *"Fluid selection and thermodynamic optimization of organic Rankine cycles for waste heat recovery applications"* **Energy Procedia *129***: 527–534. DOI: https://doi.org/10.1016/j.egypro.2017.09.180. URL: https://www.sciencedirect.com/science/article/pii/S1876610217340948.

[14] U. Larsen, L. Pierobon, F. Haglind, and C. Gabrielii, (2013) *"Design and optimisation of organic Rankine cycles for waste heat recovery in marine applications using the principles of natural selection"* **Energy *55***: 803–812. DOI: https://doi.org/10.1016/j.energy.2013.03.021. URL: https://www.sciencedirect.com/science/article/pii/S0360544213002090.

[15] D. H. Wolpert, (1992) *"Stacked generalization"* **Neural Networks *5***(2): 241–259. DOI: https://doi.org/10.1016/S0893-6080(05)80023-1. URL: https://www.sciencedirect.com/science/article/pii/S0893608005800231.

[16] K. Deb, A. Pratap, S. Agarwal, and T. Meyarivan, (2002) *"A fast and elitist multiobjective genetic algorithm: NSGA-II"* **IEEE Transactions on Evolutionary Computation *6***(2): 182–197. DOI: 10.1109/4235.996017.

[17] X. Zhao, H. Chen, S. Li, W. Li, P. Pan, T. Liu, L. Wu, and G. Xu, (2023) *"Thermodynamic and economic analysis of a novel design combining waste tire pyrolysis with silicon production waste heat recovery and organic Rankine cycle"* **Energy *283***: 128500. DOI: https://doi.org/10.1016/j.energy.2023.128500. URL: https://www.sciencedirect.com/science/article/pii/S0360544223018947.

[18] Q. Wu, Q. Zhang, X. Chen, G. Song, and J. Xiao, (2022) *"Integrated Assessment of Waste Tire Pyrolysis and Upgrading Pathways for Production of High-Value Products"* **ACS Omega *7***(35): 30954–30966. DOI: 10.1021/acsomega.2c02952. URL: https://doi.org/10.1021/acsomega.2c02952.

[19] L. Pierobon, M. Rokni, U. Larsen, and F. Haglind, (2013) *"Thermodynamic analysis of an integrated gasification solid oxide fuel cell plant combined with an organic Rankine cycle"* **Renewable Energy *60***: 226–234. DOI: https://doi.org/10.1016/j.renene.2013.05.021. URL: https://www.sciencedirect.com/science/article/pii/S0960148113002668.

[20] Taiwan Power Company. *Sustainability Report: Carbon Emission Factor of Electricity Grid in Taiwan*. 2024. URL: https://www.taipower.com.tw/.